Chapter 5

Synthesis of Clove essential oil functionalized gold nanoparticles and their antibacterial, antioxidant, anticancerous and biocompatibility responses

5.1Introduction

Owing to widespread involvement in several pharmaceutical and food items, as well as their potential to suppress the growth and spread of a variety of microbes, including bacteria, fungus, and viruses, essential oils (EOs) have been significantly seeking attention in recent years (Chami et al., 2005; Chaieb et al., 2007; Fu et al., 2007). The general physicochemical properties (complexity and interactions of distinct compounds) and components (low molecular weight, presence of several functional groups in the molecule, reactivity, and hydrophobicity) of EOs have a significant impact on their biological activity. The family of Myrtaceae plant, *Syzygium aromaticum L.*, produce clove essential oil (CEO), an essential oil which is used to treat a wide range of diseases (Chaieb et al., 2007; Fu et al., 2007; Cai et al., 1996). There have been various pharmacological bioactivities reported for CEO, including anti-inflammatory, analgesic, antibacterial, antifungal, anti-allergic, anti-carcinogenic, and anti-mutagenic activities (Chami et al., 2005; Zheng et al., 1992; Beuchat et al., 2007; Miyazawa et al., 2001; Friedman et al., 2002; Cressy et al., 2003; Kalemba et al., 2003). Several phytochemicals

have been found in CEO such as eugenol, acetyleugenol, isoeugenol, methy- leugenol, carvacrol, thymol, cinnamaldehyde, eugenyl acetate, β-caryophyllene, 2-heptanone, methyl salicylate, α-humulene, gallic acid, ellagic acid and oleanolic acid etc (Chaieb et al., 2007; Fu et al., 2007; Cai et al., 1996). Eugenol（88.58%）is the major constituent of CEO which displays significant anti-oxidant and insecticidal properties (Chaieb et al., 2007; Fu et al., 2007; Friedman et al., 2002; Cressy et al., 2003; Kalemba et al., 2003; Ogata et al., 2000; Park et al., 2000). Eugenol is an associate with the allylbenzene class of aromatic substances and is an almost pale or colourless oily liquid with an aromatic ring (Cortés-Rojas et al., 2014; Mallavarapu et al., 1995). It is used as an antiseptic, anesthetic, antibacterial, and antifungal agent (Rastogi et al., 2013). It has been reported that the eugenol has the potentiality to disintegrate in the membrane and enhance its permeability, which subsequently causes death of the organism (Gill et al., 2006). Since eugenol is unstable in aqueous solution and lipophilic, it has been rapidly absorbed into the lipid bilayer of mammalian cell membranes (Atsumi et al., 2001). The literature also reported that eugenol likely to possess a protective role in healthy cells while enhancing cytotoxicity in cancerous cells (Wie et al., 1997; Yoo et al., 2005). Several encapsulation techniques for EOs, such as metallic nanoparticles, inorganic nanoparticles, solid lipid nanoparticles, nanogels, polymeric nanoparticles, silica nanoparticles and liposomes, are currently the focus of scientific research with the ultimate objective of obscuring their undesirable properties and enhancing their biological activities. Nano-encapsulation is one of the most effective and powerful techniques for protecting EOs and bioactive components from direct contact with the environment. Additionally, encapsulation lessens the volatility and toxicity of EOs by enhancing their surface-to-volume ratio, facilitating controlled and site-specific distribution as well as deep tissue penetration. On

contrary to pure essential oils, which have a poor water solubility and are unable to penetrate bacterial cell membranes, studies indicate that nano-encapsulation can carry essential oils to the surface of bacterial cell membranes and improve their absorption (Mohammadi et al., 2020). A range of nanomaterial, including gold, silver, platinum, iron, copper, chitosan, and zinc, have been employed in the production of EO-loaded NPs with outstanding antibacterial properties in order to get beyond the limitation of EOs. The life span of the final product is increased by nanoparticles' safeguarding of EOs from heat and UV destruction, which results in improved stability, flavour retention, and function. Additionally, for prolonged therapeutic effects, NPs provide regulated release of EOs. By improving the ability of essential oils to diffuse through biological membranes, essential oil-loaded nanoparticles (NPs) exhibit synergistic antibacterial effect. Therefore, the objective of the present study is to fabricate and characterize the CEO-*f*AuNP in order to investigate its multifunctional properties, including antibacterial, antioxidant, anticancerous, and biocompatibility. To distribute and release the antimicrobial agent in a controlled way utilising nanometric vehicles is a promising approach.

We utilized PEI-based AuNPs synthesized in our laboratory for this purpose (Pandey et al., 2023; Pandey et al., 2016). According to reports, polymers such as polyethylenimine (PEI) contributes to the regulated synthesis of AuNPs in normal conditions, it may facilitate specific interactions with DNA-binding proteins (Pandey et al., 2016). PEI, a cationic polymer mentioned earlier, is crucial for rapidly converting gold cations into AuNPs and creating a cationic coating for drug loading (Pandey et al., 2016). PEI serves multiple functions, including imparting a positive charge to nanoparticles, regulating their size, and stabilizing them; (Mohammed et al., 2013).PEI can efficiently stabilise a variety of nanoparticles, including metal and metal oxide nanoparticles, due to the

substantial presence of primary amino groups in it (Wen et al., 2013; Lee et al., 2011). Furthermore, it contributes to the regulation of gold nanoparticles maturation by providing surface shielding (Mohammed et al., 2013). Moreover, this chapter describes the synthesis of highly stable CEO-*f*AuNP, which can disperse in water, and evaluates its potential as an antibacterial, antioxidant, and cancer-preventive agent through in vitro cytotoxicity testing. The nano-synthesis process is monitored using UV-vis spectrometry. The characterization of the synthesized conjugated nanoparticles involves the utilization of techniques such as X-ray diffraction (XRD), Fourier-transform infrared spectroscopy (FTIR), transmission electron microscopy (TEM), dynamic light scattering (DLS), and zeta potential analysis. These techniques enable the assessment of the crystalline nature, surface coating, size, shape, and elemental composition of the nanoparticles. This study provides a detailed description of the sophisticated and well-defined synthesis process employed for CEO-*f*AuNP, showcasing its noteworthy stability at room temperature for duration of 8-9 months. The formation mechanism of the crystalline and spherical CEO-*f*AuNP is elucidated through the application of high-resolution transmission electron microscopy (HRTEM) and absorbance spectroscopy, confirming the robust conformation of CEO-*f*AuNP. Furthermore, the research investigates the effects of CEO-*f*AuNP on antibacterial activity and cellular response, providing valuable insights into the impact of functionalized nanoparticles. Considering the limited research on the antibacterial activity and mode of action of CEO against MDR bacteria, this chapter provides a comprehensive understanding and further validation of CEO as an effective antibacterial, antioxidant, and anticancer agent that is also biocompatible.

5.2 Results and discussion

The synthesized CEO-*f*AuNPs were characterized using UV-Vis spectroscopy and transmission electron microscopy (TEM). The phase evolution, microstructure analysis,

Dynamic Light Scattering (DLS) and Zeta potential, antibacterial, and cytocompatibility results are described in subsequent sections.

5.2.1 UV-Vis absorbance Spectroscopy

Table 5.1 and Figure 5.1 present the spectra of CEO-*f*AuNP compared to AuNPs at different time intervals (15 min, 30 min, 60 min, 120 min, and overnight) for different CEO concentration (b-e). Figure 1(f) displays the typical spectra of CEO and CEO-*f*AuNP after six months. The UV spectra of CEO and AuNPs exhibit the highest absorption at 280 nm and 520 nm, respectively.

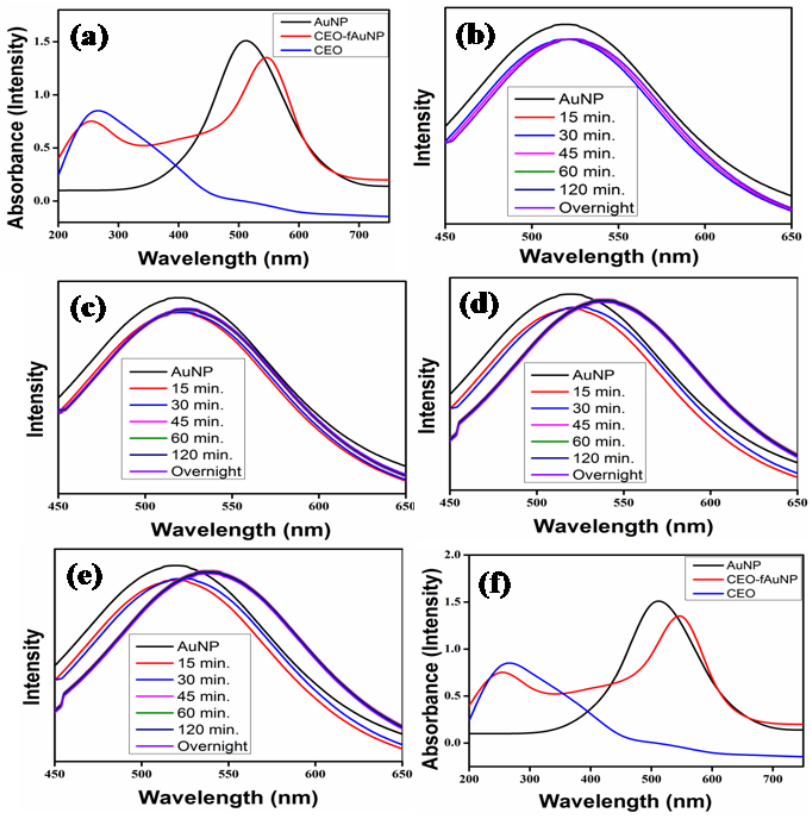

Figure 5.1 *Representing (a) UV-vis absorbance Spectrometry of CEO, AuNP and CEO-fAuNP, (b-e) absorbance spectra of CEO-fAuNPs with different CEO conc. compared with AuNPs spectra, (f) absorbance spectra of CEO, AuNP and CEO-fAuNP after six months*

The absorption analysis of CEO-*f*AuNP (50 µL CEO, 45 min) indicates an optimal plasma resonance wavelength of 539 nm with a minor peak at 280 nm (Figure 5.1(a)). The observed peak shift from 520 nm to 539 nm provides evidence for the interaction between AuNPs and CEO

Table 5.1 *Analysis of λmax of CEO-fAuNP with respect to time and different CEO concentration.*

S. No.	**AuNPs (µL)**	**CEO (µL)**	**Time (** min)	**λmax (approximately)**
1	100	10	15	520
			30	520
			45	522
			60	523
			120	523
			Overnight	523
2	100	20	15	520
			30	522
			45	525
			60	525
			120	525
			Overnight	525
3	100	50	15	520
			30	525
			45	539
			60	539
			120	539
			Overnight	539
4	100	100	15	520
			30	525
			45	539
			60	539
			120	539
			Overnight	539

The optimal conditions for functionalization involve mixing 50 µL of CEO with 100 µL of AuNPs for 45 min at room temperature. The surface plasmon absorbance remains largely unaffected by mixing time or concentration.

Furthermore, the stability of CEO-*f*AuNP at ambient temperature is demonstrated by the persistence of the plasmon absorbance band centered at 539 nm even after 6 months (Figure 5.1 e), albeit with a slight decrease in absorbance and no wavelength shift. The red shift in the CEO-*f*AuNP spectrum indicates surface changes resulting from CEO modification. The prominent absorption peak of AuNPs, located around 520 nm, is attributed to the collective electron oscillation phenomenon called plasmon resonance (Pandey et al., 2023). The presence of a minor absorption band at approximately 280 nm in the CEO-*f*AuNP spectrum corresponds to the characteristic absorption of CEO, indicating successful functionalization. Moreover, no noticeable alterations are observed in the spectra at 280 nm.

5.2.2 Dynamic Light Scattering (DLS) and Zeta potential

Table 5.2 presents the DLS, polydispersity index (PDI) and Zeta potential data for CEO-*f*AuNP and AuNPs. The hydrodynamic size of CEO-*f*AuNP was determined to be 65.38 nm [Figure 5.2(a)], while for AuNPs; it measured approximately 40.2 nm [Figure 5.2(b)]. The incorporation of CEO into the gold nanoparticle surface is likely responsible for this size enhancement. The PDI values of AuNP and CEO-*f*AuNP fell within the range of 0.262 to 0.313. A lower value indicates a more efficient and even dispersion of nanoparticles throughout the solution.

Table 5.2. *Dynamic light scattering (DLS), polydispersity index and zeta potential for AuNPs and CEO-fAuNP sample.*

Sample	**Average Size (nm)**	**Polydispersity Index**	**Zeta (mV)**
AuNP	40.20 ± 2.1	0.262 ± 0.012	38 ± 0.7
CEO-*f*AuNP	65.38 ± 2.5	0.313 ± 0.017	-30 ± 0.11

The Zeta potential measurements indicate a strongly positive/negative surface charge for the two systems, with values of 38 mV [Figure 5.3(a)] for AuNPs and -30 mV [Figure 5.3(b)] for CEO-*f*AuNP suspensions, suggesting their electrostatic stability.

The surface charge of AuNPs has been reduced as a result of functionalizing them with CEO, thus demonstrating the capability of CEO to modulate the surface structure. Studies have found that the generation of a physically stable nanosuspension by electrostatically stabilised particles requires a zeta potential of at least 30 mV (Kamble et al., 2010; de Oliveira et al., 2022).

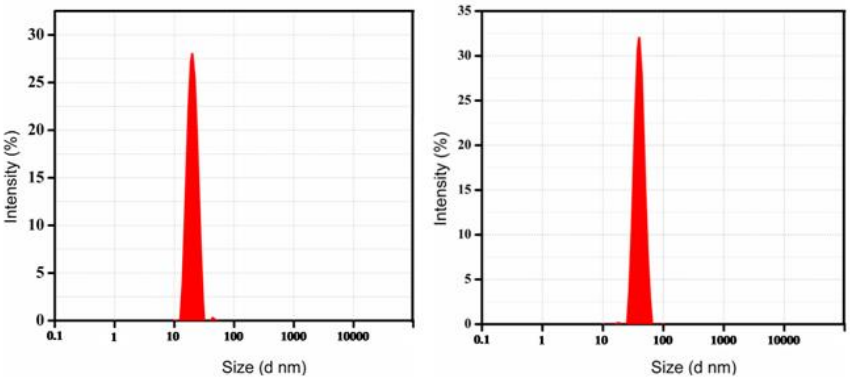

Figure 5.2 *Hydrodynamic diameters of (a) AuNP and (b) CEO-fAuNP*

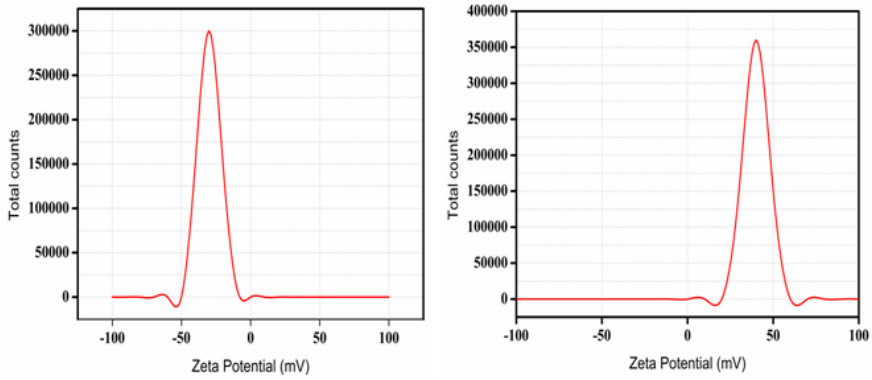

Figure 5.3 *Zeta potential of CEO-fAuNP (a) and AuNP (b)*

Less aggregation and excellent stability with extended storage are attributed to a negative surface charge (Pandey et al., 2023). For six months, CEO-*f*AuNP is observed stable. The

spectroscopic attributes (colour, texture, etc.) remained unchanged during this time of preservation.

5.2.3 Phase evolution and microstructural analysis

The phase evolution of synthesized AuNPs, CEO and CEO-*f*AuNP are shown by the XRD patterns (Figure 5.4). At 38.18°, 44.37°, 64.48°, and 77.37°, considerable diffraction peaks are clearly visible which attribute to crystal planes of the cubic phase metallic AuNPs (111), (200), (220), and (311) (JCPDS no. 04-0784) (Pandey et al., 2023). A broad peak has been observed for CEO within the range of 11.45°–13.35°. There are no sharp peaks due to viscous liquid in structure (Hameed et al., 2021). No significant change has been observed in crystallanity of AuNP after incorporation of CEO in case of CEO-*f*AuNP (Figure 5.4).

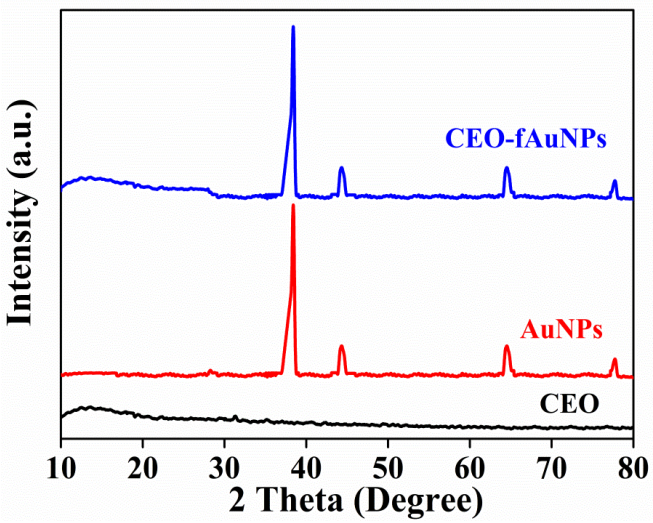

Figure 5.4 *X-ray diffraction (XRD) pattern of CEO, AuNPs and CEO-fAuNPs*

To detect the functional groups present in CEO-*f*AuNP, FTIR analysis was done (Figure 5.5). The characteristic bands found in CEO are as follows: a wide band at 3300-3400 cm^{-1} attributed to phenolic and aliphatic –OH groups, followed by bands at 1645 cm^{-1} attributed to C-H stretching vibration of benzene, at 1379 cm^{-1} was the C-H deformation vibration of eugenol methyl, at 1715 cm^{-1} was C=O stretching vibration of carboxylic

acid, at 1265 cm^{-1} was the C-O stretching vibration of phenolic hydroxyl, and at 1039 cm^{-1} was the C-O-C stretching vibration of aromatic ether.

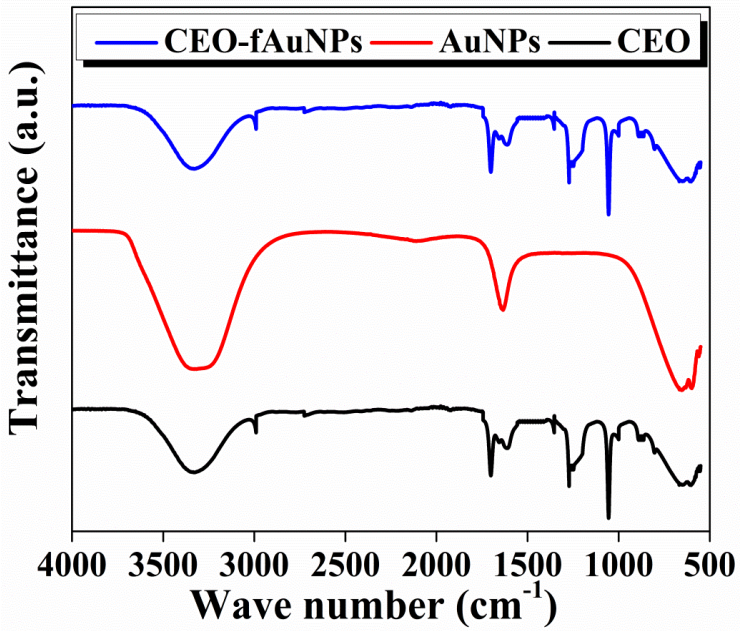

Figure 5.5 *Fourier transform infrared spectroscopy (FTIR) spectra of CEO, AuNPs and CEO-fAuNPs*

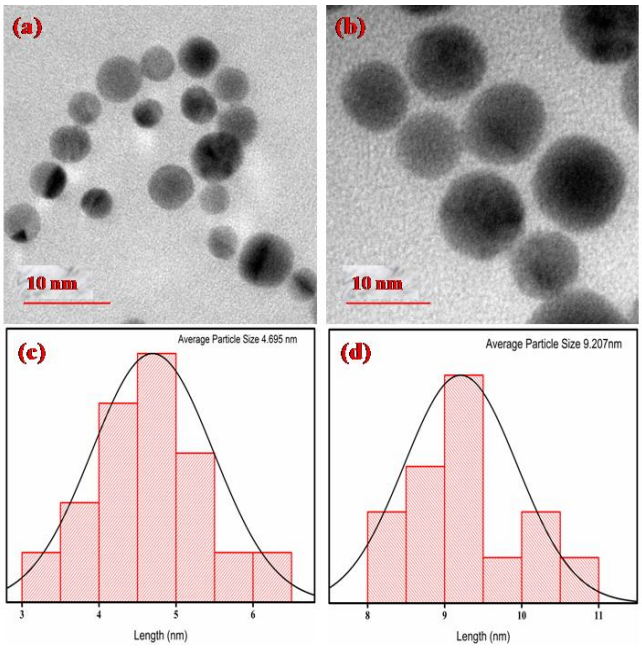

Figure 5.6 *TEM images of AuNP (a), CEO-fAuNP (b) and their respective size distribution histogram (c) & (d)*

The FTIR spectrum of the CEO-*f*AuNP was almost similar to that of CEO, which was due to surface functionalization AuNP with CEO. However, the absorption peak of – OH groups were observed at 3310 cm^{-1} in the FTIR spectrum, and the significant shift (30 cm^{-1}) implied strongly the hydrogen bonding interaction between CEO and PEI coated AuNP.

Figure 5.6 represents the TEM image and size distribution histogram of AuNP (5.6a & 5.6c) and CEO-*f*AuNP (5.6b & 5.6d). In case of AuNP; TEM images demonstrate the spherical shaped particles with an average diameter of ~4.7 nm while for CEO-*f*AuNP the particles size was increased to ~9.2 nm. The histogram plot was obtained using image-J software, by measuring the diameter of approximately 50-60 nanoparticles and the statistical analysis was done on Origin, which resembled different-sized particles with a size distribution window in the range of 3-7 nm (AuNP) and 8-11 nm (CEO-*f*AuNP). The surface functionalization of CEO on AuNP is further supported by the increase in size of CEO-*f*AuNP then AuNP (Pandey et al., 2023).

5.2.4. Antibacterial effect

5.2.4.1. Minimum inhibitory concentration (MIC) determination

Figure 5.7 shows the MIC of CEO and CEO-*f*AuNP against *Klebsiella pneumoniae* using broth micro-dilution assay. The optimum MIC is observed for CEO (256 µg/ml) than AuNPs (32 µg/ml) and CEO-*f*AuNP (0.5 µg/ml), which aligned with the conclusions of the other research. It is observed that CEO-*f*AuNP exhibit the lowest MIC 0.5 µg/ml, which consequently indicating that functionalization of CEO with AuNPs significantly escalates its bactericidal potential.

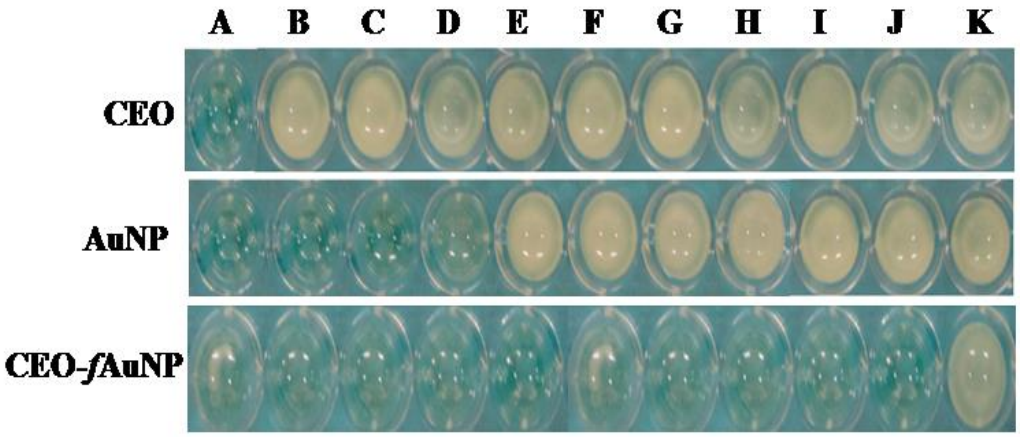

Figure 5.7 *MIC determination by the microbroth dilution method: CEO treated (256 µg mL^{-1}), AuNP treated (32 µg mL^{-1}) and CEO-fAuNP treated (0.5 µg mL^{-1}). Wells A-K containing serially doubly-diluted test compounds ranging from 256 µg mL^{-1} (well A) to 0.25 µg mL^{-1} (well K)*

5.2.4.2. Antibiofilm activity determination

During the investigation of the inhibitory impact of AuNPs, CEO, and CEO-*f*AuNP (MIC concentration) on antecedently formed biofilms, the results showed that CEO-*f*AuNP treatment resulted in approximately 89% inhibition.

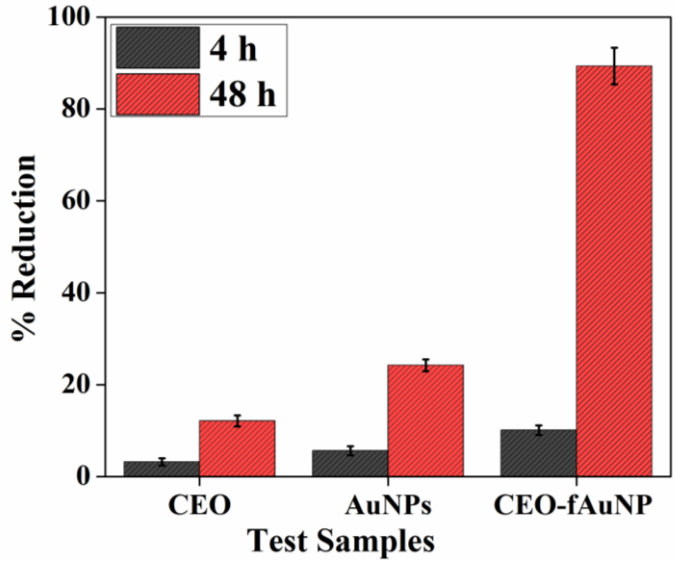

Figure 5.8 *Crystal violet based antibiofilm assay. Plot depicting absorbance readings with different test samples at 4 and 48 h.*

In comparison, CEO alone and AuNPs individually fostered around 10% and 24% inhibition of biofilms, respectively (Figure 5.8). Initially, all the test compounds had negligible effects. However, at a later time point (48 h), CEO-*f*AuNP exhibited significant effectiveness, surpassing both CEO and AuNPs when used independently.

5.2.4.3. Bacterial growth reduction analysis

The bacterial growth reduction has been observed using time-kill analysis. It is observed that CEO and CEO-*f*AuNP exhibited a strong bactericidal effect on MDR bacteria Treatment with MIC conc. and consequently, within 20 h the bacterial population was completely inactivated (Figure 5.9). In addition, prolonged exposure to CEO-*f*AuNP results in loss of viability. These findings indicate that within 20 hours of exposure, CEO-*f*AuNP substantially inhibits the MDR bacteria's ability to proliferate.

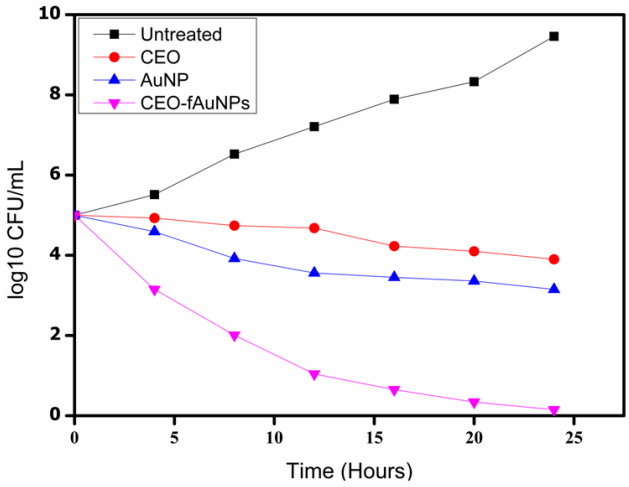

Figure 5.9 *Kill curves for log-phase growing multi-drug resistant Klebsiella pneumoniae treated with MIC concentration of CEO (128 µg/ml), AuNP (32 µg/ml), CEO-fAuNP (8 µg/ml) compared with untreated*

5.2.5. Antioxidant activity (DPPH free radical assay)

A standard DPPH free radical assay has been used to assess the antioxidant activity of AuNPs, CEO and CEO-*f*AuNP (MIC conc.). It is clearly observed by the Figure 5.10 that

the absorption peak of DPPH radicals (at 517 nm) is decreases after addition of CEO in AuNP reaction mixture.

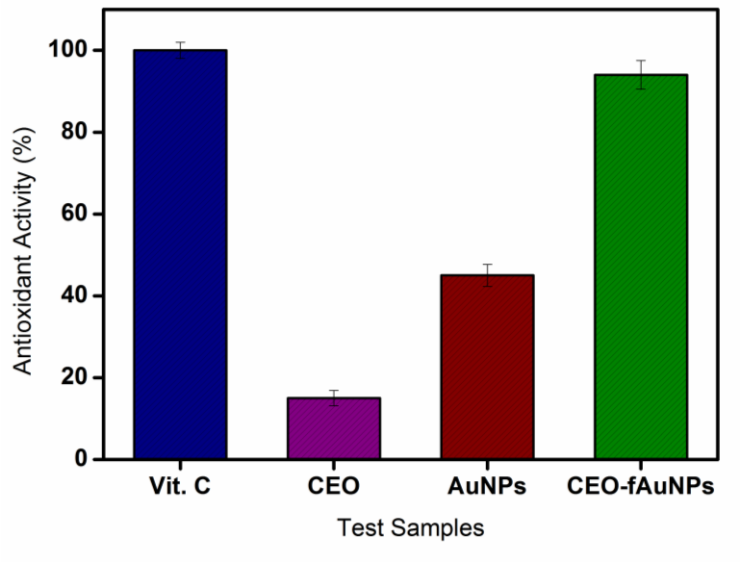

Figure 5.10 *Antioxidant activity of CEO, AuNP , CEO-fAuNP compared with antioxidant activity of Vit. C*

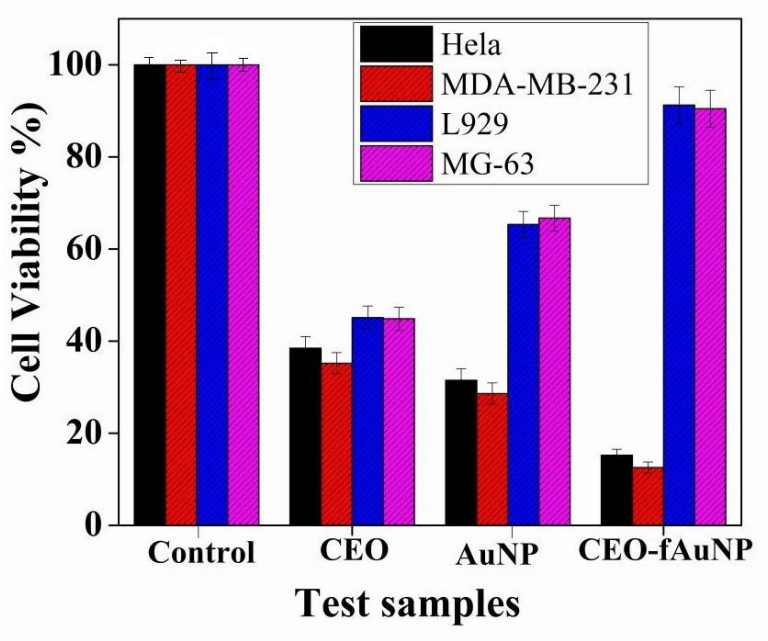

Figure 5.11 *Cytotoxicity results for Hela, MDA-M-231, L929 and Mg-63 cell lines treated with different test samples*

5.2.6. Anti-cancerous activity

MTT assay has been use to observed the anti-proliferative effect of the optimized CEO-*f*AuNP. It has been observed by MTT result that the fabricated clove conjugated AuNPs expressed cytotoxicity against Hela and MDA-MB-231 cancer cell lines. Figure 5.11 shows the variation in cell viability of Hela and MDA-MB-231 cancer cell lines treated with AuNPs, CEO and CEO-*f*AuNP and untreated cells.

5.2.7. Biocompatibility

The cytocompatibility test has been performed to observe the effects of the AuNPs, CEO and CEO-*f*AuNP (MIC conc.) for possible toxicity to mammalian systems. MTT assay is one of the methods to measure the biocompatibility (quantitatively). In this study, MG-63 and L929 cell lines are used to investigate the in vitro toxicity of AuNPs, CEO and CEO-*f*AuNP.

The results indicate that the direct interaction with the fabricated nanoparticle samples does not seem to negatively affect the viability of both cell types. Figure 5.11 illustrates the changes in cell viability for MG-63 and L929 cells when treated with AuNPs, CEO, and CEO-*f*AuNP, as well as untreated cells. The statistical analysis clearly demonstrates that the treated cells exhibit a noticeable disparity in mean optical density compared to the untreated cells.

In addition, cultured cells that have been incubated for 5 and 7 days compared to those that have incubated for 3 days show a statistically significant increase in cell proliferation, regardless of treatment. Furthermore, in comparison to CEO and AuNPs treatment, CEO-fAuNP treatment accelerates cell proliferation. Therefore, it can be concluded that, in contrast to CEO and AuNPs independently CEO functionalized AuNPs significantly enhances cell growth and proliferation.

5.3 Conclusion

In this chapter, synthesis of clove conjugated gold nanoparticles (CEO-*f*AuNP) using polyethylenimine (PEI) have been demostrated. Preliminary characterizations such as UV-Vis spectroscopy, XRD and FTIR reveal the formation of conjugated CEO-*f*AuNP. The zeta potential value shows the stability of colloidal solution of CEO-*f*AuNP. In conclusion, we have provided an easy approach for functionalizing CEO with AuNPs, which are extremely stable in aqueous medium at ambient temperature. The plasmon resonance signature of gold remains intact after functionalization ensuring the bio-active nature of CEO and gold signature. Additionally, the synthesized CEO-*f*AuNP demonstrated outstanding antibacterial, antibiofilm, antioxidant, and anticancerous properties. In order to ensure the biocompatibility of as synthesized CEO-*f*AuNP, we further examined its biosafety profile using cell culture (MG-63 and L929 cell line). The zeta potential on the surface of AuNPs and CEO-*f*AuNP was more than ±25 mV which is a sign of their high stability. The CEO-*f*AuNPs also demonstrated selective synergistic toxicity on bacteria (*Klebsiella pneumoniae*) as opposed to mammalian cells (MG-63 cell line), and the sharp drop in MIC of AuNPs following CEO functionalization suggests that CEO-*f*AuNPs may be suitable for systemic medical application. These experiments suggest that the synthesized CEO-*f*AuNP could be suitable for a range of biomedical applications.